Hindawi
International Journal of Photoenergy
Volume 2018, Article ID 8715987, 9 pages
https://doi.org/10.1155/2018/8715987

Research Article

Photocatalytic Activity under Simulated Sunlight of Bi-Modified TiO_2 Thin Films Obtained by Sol Gel

D. A. Solís-Casados,[1] **L. Escobar-Alarcón**,[2] **V. Alvarado-Pérez**,[1] **and E. Haro-Poniatowski**[3]

[1]*Universidad Autónoma del Estado de México, Centro Conjunto de Investigación en Química Sustentable UAEMéx-UNAM, Toluca, MEX, Mexico*
[2]*Departamento de Física, Instituto Nacional de Investigaciones Nucleares, Apartado Postal 18-1027, 11801 Mexico City, Mexico*
[3]*Departamento de Física, Universidad Autónoma Metropolitana, Apartado Postal 55-532, 09340 Mexico City, Mexico*

Correspondence should be addressed to D. A. Solís-Casados; solis_casados@yahoo.com.mx

Received 20 July 2017; Revised 27 October 2017; Accepted 13 December 2017; Published 19 March 2018

Academic Editor: Juan Rodriguez

The synthesis of Bi-modified TiO_2 thin films, with different Bi contents, is reported. The obtained materials were characterized by energy-dispersive X-ray spectroscopy (EDS), X-ray photoelectron spectroscopy (XPS), Raman spectroscopy (RS), X-ray diffraction (XRD), photoluminescence (PL), and diffuse reflectance spectroscopy (DRS), in order to obtain information on their chemical composition, vibrational features, and optical properties, respectively. Compositional characterization reveals that the bismuth content can be varied in an easy way from 0.5 to 25.4 at. %. Raman results show that the starting material corresponds to the anatase phase of crystalline TiO_2, and Bi addition promotes the formation of bismuth titanates, $Bi_2Ti_2O_7$ at Bi contents of 10.4 at. % and the $Bi_4Ti_3O_{12}$ at Bi contents of 21.5 and 25.4 at. %. Optical measurements reveal that the band gap narrows from 3.3 eV to values as low as 2.7 eV. The photocatalytic activity was tested in the degradation reaction of the Malachite Green carbinol base dye (MG) as a model molecule under simulated sunlight, where the most relevant result is that photocatalytic formulations containing bismuth showed higher catalytic activity than pure TiO_2. The higher photocatalytic activity of MG degradation of 67% reached by the photocatalytic formulation of 21.5 at. % of bismuth is attributed to the presence of the crystalline phase perovskite-type bismuth titanate, $Bi_4Ti_3O_{12}$.

1. Introduction

Pollution in wastewaters is one of the most important environmental topics nowadays due to the increasing necessity of human beings of clean water. Some dyes in wastewaters are considered pollutants and, in most cases, are considered toxic to humans and other living organisms, even when they are present in low quantities. Several processes have been proposed to remove or degrade these pollutants from wastewaters; particularly, the photocatalysis is currently considered a promising alternative to remove dyes from water in an efficient way. Photocatalysis is an advanced oxidation technology (AOT), based on physicochemical processes that produce changes in the chemical structure of the organic compounds including their mineralization. AOT processes are based on the generation and the use of highly reactive oxidizing species, such as the hydroxyl ($OH^{\bullet}$), hydroperoxyl ($^{\bullet}OOH$), and superoxide radicals ($O_2^{\bullet}$), which are reactive sites towards degradation of organic compounds until their complete mineralization [1]. Among the photocatalytic materials, titanium dioxide (TiO_2) has been the most used because of its specific properties, such as resistance to chemical corrosion, nontoxic, and inexpensive, and its high photoactivity with UV radiation. However, TiO_2 has two important drawbacks; the first one is that it is activated only by ultraviolet light, due to its relatively high band gap energy

of 3.2 eV for the anatase crystalline phase. The second one is the high recombination rate of the photogenerated electron-hole pairs that reduce its efficiency [2]. Several strategies have been proposed to improve the photocatalytic activity of TiO_2 such as doping it with metals and nonmetals, as well as the use of mixtures of the two main TiO_2 crystalline phases, anatase and rutile [3, 4]. Coupling of semiconductors has been also considered as an alternative route to develop high efficient photocatalytic materials that can compensate the disadvantages of the individual components inducing synergistic effects such as efficient charge separation, band gap narrowing, and consequently improvement of their photocatalytic performance. Therefore, the development of visible light-driven coupled photocatalysts is currently of great interest. Particularly, bismuth oxide (α-Bi_2O_3) has been reported as an efficient photocatalyst due to its unique structure and band gap energy close to 2.8 eV which makes it active in the visible region of the electromagnetic spectrum [5, 6]. Several studies have reported that the system formed by mixtures of TiO_2 and Bi_2O_3 can result in the formation of different crystalline phases of bismuth titanates ($Bi_4Ti_3O_{12}$ and $Bi_{12}TiO_{20}$) depending on the proportion of TiO_2 and Bi_2O_3 [7, 8]. It is worth mentioning that the photocatalysts based on $Bi_{12}TiO_{20}$ [9] and $Bi_4Ti_3O_{12}$ [10] crystals have been tested in the photodecolorization of methyl orange under UV irradiation showing high photocatalytic activity, similar in both cases. The aim of this work is to investigate the degradation of the Malachite Green dye (MG), carbinol base, under visible light irradiation, using a simulated sunlight source, in an attempt to correlate the photocatalytic activity of titanium oxide modified with different amounts of Bi_2O_3 with their physicochemical properties in particular; the band gap energy, the microstructure, and the electron-hole recombination rate.

2. Experimental

2.1. Bi-Modified TiO_2 Thin Films. The precursor solutions were prepared by the sol-gel technique. Titanium isopropoxide ($Ti[OCH(CH_3)_2]_4$, Aldrich 97%), nitric acid (HNO_3, Fermont 70%), 2-propanol ($CH_3CHOHCH_3$, Fermont 99.8%), bismuth nitrate pentahydrate ($Bi(NO_3)_3{\bullet}5H_2O$, J.T. Baker) were used as precursors. A sol was prepared under environmental conditions mixing 10 mL of 2-propanol with 1 mL of titanium isopropoxide, stirred for 1 h. Bismuth nitrate pentahydrate was added slowly under stirring to obtain theoretical amounts of 0, 5, 30, 50, 70, and 80 wt. % of Bi_2O_3. 1 mL of nitric acid was added drop to drop to induce gelling as a variant of the sol-gel technique reported before [11]. The sol was sonicated in an ultrasonic bath during 5 min and aged for 12 h to obtain an incipient gelled solution. Afterwards, the precursor solution was deposited layer to layer by the spin coating technique onto borosilicate glass substrates (25 mm × 25 mm × 1 mm) functionalized with hydrofluoric acid (HF, 10% vol) to obtain homogeneous thin films. The spin coater was a KW-4A from Chemat Technology working at 1500 rpm under environmental conditions. Deposited thin films were thermally treated at 300°C during 1 h to eliminate organic residues, and subsequently, the temperature was raised to 450°C at a heating rate of 3°C/min and maintained isothermally for 4 h to form a crystalline thin film.

2.2. Thin Film Characterization. Determination of the atomic bismuth content in the films was done by energy-dispersive X-ray spectroscopy (EDS) using a microprobe attached to a JEOL JSM 6510LV scanning electron microscope, and EDS analysis was carried out with an acceleration voltage of 15 kV; surface morphology was observed from micrographs obtained with the same microscope. The chemical bonding of the present elements was investigated by X-ray photoelectron spectroscopy (XPS). The wide and narrow XPS spectra were acquired using a JEOL JPS-9200 spectrometer. The adventitious carbon peak at 284.8 eV (1s) was used as the internal standard to compensate for sample charging. Raman spectroscopy (RS) was used to study the structural features of the films; spectra were acquired using an HR LabRam 800 spectrometer with an Olympus BX40 confocal microscope. A Nd:YAG laser beam (532 nm) was focused with a 50x objective onto the sample surface. A cooled CCD camera was used to record the spectra, and typically, an average of 50 accumulations of 10 seconds was done to improve the signal-to-noise ratio. The crystalline phases of the thin films were identified by the X-ray diffraction technique (XRD) with a Bruker D8 Advance Diffractometer using the Cu-Kα radiation line ($\lambda = 1.54$ Å); the diffraction patterns were recorded in steps of 0.05°. Diffuse reflectance spectroscopy (DRS) spectra were acquired on a PerkinElmer Lambda 35 spectrophotometer with an integration sphere with a resolution of ±1 nm; from the reflectance spectra, the Kubelka-Munk function was determined and the band gap energy was estimated [12, 13]. Photoluminescence spectra were acquired in a FluoroMax4, HORIBA Jobin Yvon spectrofluorometer, exciting the samples at 492 nm.

2.3. Photocatalytic Activity. The photocatalytic activity of the thin films was tested through the degradation of Malachite Green carbinol base dye ($C_{23}H_{26}N_2O$, Aldrich) contained in an aqueous solution (10 μmol/L). The reaction was carried out in a batch system in a borosilicate glass reactor, in which the thin film was introduced into a 25 mL of the MG solution; afterwards, the reaction system was stirred in dark condition in order to establish adsorption equilibrium between dye solution and photocatalyst. Thin films were activated by illumination with light emitted from a solar simulator SF150 of Sciencetech equipped with an AM1.0D filter which simulates the solar spectrum of direct light from the sun on the ground when the sun is at a zenith angle of 0°; the samples were irradiated with an average intensity of 60 mW/cm^2 keeping the distance between the liquid surface and the light source at 15 cm. The MG photodegradation was followed through the decrease of its characteristic absorption band peaking at 619 nm in the UV-Vis absorbance spectra. The spectra were obtained each 15 min in the first hour of reaction time, and afterwards, each 30 min during the second and third hours of reaction from the aliquots of 4 mL taken from reaction system and were returned to the reactor after each spectrum was taken. Absorbances obtained at each reaction time were

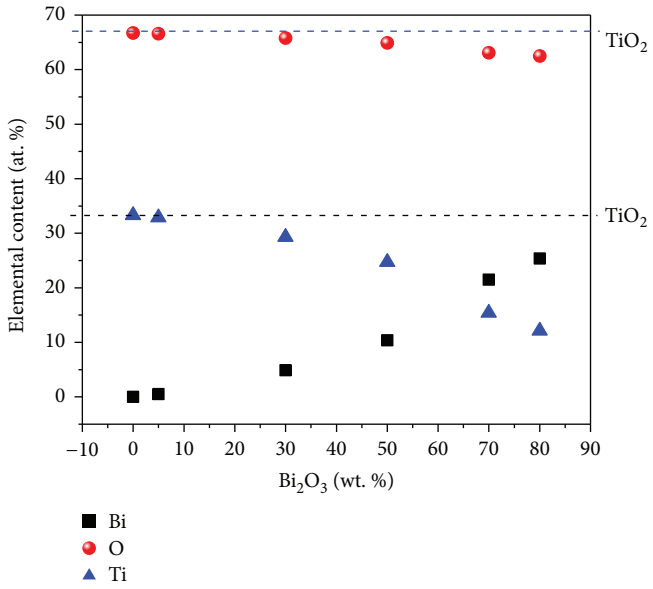

Figure 1: Atomic proportion of the thin films as a function of the Bi_2O_3 wt. %.

correlated to dye concentrations through a calibration curve. A nonlinear least square data treatment was used to determine the values of the kinetic constant considering a pseudo-first order kinetic model. Total organic carbon (TOC) was determined in each solution after reaction as ppm of carbon, TOC was obtained by the combustion method, and the mineralization degree was calculated taking the TOC content in the MG solution, at the initial concentration of 10 μmol/L, 9.2 ppm of TOC as a reference.

3. Results and Discussion

3.1. Elemental Composition. The elemental chemical composition of the deposited thin films, as a function of the Bi_2O_3 wt. % used for their preparation, is shown in Figure 1 and Table 1 (EDS measurements). The results obtained from the EDS and XPS techniques showed good agreement following the same tendency. It is clearly observed that the film without Bi is almost stoichiometric TiO_2. When Bi is incorporated increasing the Bi_2O_3 load, the Bi content in the film increases monotonically from 0.5 to 25.4 at. % whereas the O content remains around 65 at. %. Simultaneously, the Ti content decreases from 33 to 12 at. %. It is worth noting that the elemental composition of the sample prepared using 70 wt. % of Bi_2O_3 (Bi = 21.5 at. %, Ti = 15.4 at. %, and O = 63.1 at. %) agrees very well with the composition of the $Bi_4Ti_3O_{12}$ titanate (Bi = 21.0 at. %, Ti = 15.8 at. %, and O = 63.2 at. %).

3.2. Raman Spectroscopy. Figure 2 shows the Raman spectra corresponding to the thin films containing different bismuth contents, from 0.0 to 25.4 at. %. For Bi contents lower than 4.9 at. %, the spectra consist of four characteristic bands located at 144, 396, 516, and 637 cm^{-1} attributed to the anatase crystalline phase of TiO_2 [14]. The inset in Figure 2 reveals that as the Bi content increases, the band at 144 cm^{-1} shifts to higher frequencies and its intensity diminishes, and at the same time, its FWHM becomes wider. These changes are attributed to structural disorder induced by the incorporation of bismuth into the TiO_2 lattice. When the Bi content reaches 10.4 at. %, low intensity peaks associated to the anatase crystalline phase remain and new features appear at 83, 105, 256, 401, and 530 cm^{-1}, these signals that appear shifted and broader can be assigned to the bismuth titanate $Bi_4Ti_3O_{12}$ [9]. These spectra resemble an amorphous material indicating a high degree of structural disorder. At the highest Bi content, the Raman spectrum is characterized by signals at 235, 276, 350, 540, 615, and 856 cm^{-1}; the presence of the Raman modes at 276, 540, and 856 cm^{-1} suggests the presence of the perovskite structure [9].

Table 1: Elemental chemical composition, determined by EDS, of the thin films as a function of the theoretical Bi_2O_3 (wt. %).

Chemical composition (at. %)			
Bi_2O_3 (wt. %)	EDS		
	Ti	O	Bi
0	33.3	66.7	0
5	32.9	66.6	0.5
30	29.3	65.8	4.9
50	24.7	64.9	10.4
70	15.4	63.1	21.5
80	12.1	62.5	25.4

3.3. X-Ray Diffraction. Figure 3 shows the X-ray diffraction patterns from 20 to 40° of the samples with different Bi content. From Figure 3(a), the diffraction lines at $2\theta = 25.3$ and 37.8° characteristic of the TiO_2 in its anatase crystalline phase can be observed (JCPDS 89-4921). Small features of the anatase crystalline phase are observed as well (Figure 3(b)), in thin film containing 0.5 at. % of Bi. The film with bismuth content of 4.9 at. % shows diffraction lines at $2\theta =$ 14.9, 28.7, 29.96, 32.3, 34.74, and 38.01° which are attributed to the bismuth titanate $Bi_2Ti_2O_7$ (JCPDS 32-0118) (Figure 3(c)). The film containing 10.4 at. % of Bi exhibits the same diffraction lines as is seen in Figure 3(d). Further increase in bismuth content up to 21.5 at. % shows new diffraction lines peaking at $2\theta = 22.1$, 23.3, 27.2, 29.46, 30.1, and 33.1° (Figure 3(e)), characteristics of the crystalline phase of bismuth titanate with molecular structure $Bi_4Ti_3O_{12}$ (JCPDS 35-0795) as is expected because of its elemental composition. From Figure 3(f), it can be observed that crystalline phase $Bi_4Ti_3O_{12}$ remains in the thin film with 25.4 at. % of bismuth content in good agreement with the Raman results.

3.4. X-Ray Photoelectron Spectroscopy. Shifts in the peak positions in photoelectron spectra are frequently used to determine the chemical state of elements if the shifts are large enough. Sometimes, peaks representing different chemical states are overlapped and a deconvolution procedure is required. Figure 4 shows the chemical shifts of the Ti 2p region in the XPS spectra of the Bi-modified TiO_2 thin films. Spectra were deconvoluted using Gaussian functions in order

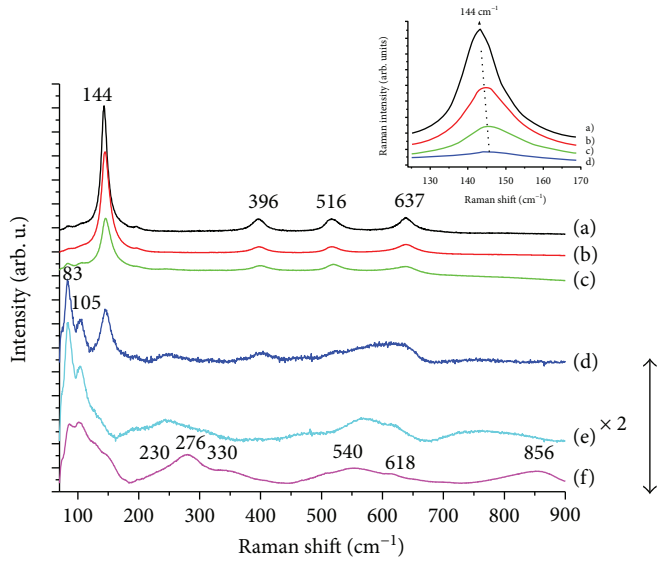

Figure 2: Raman spectra of the TiO_2 thin films modified with several bismuth contents of (a) 0, (b) 0.5, (c) 4.9, (d) 10.4, (e) 21.5, and (f) 25.4 at. %.

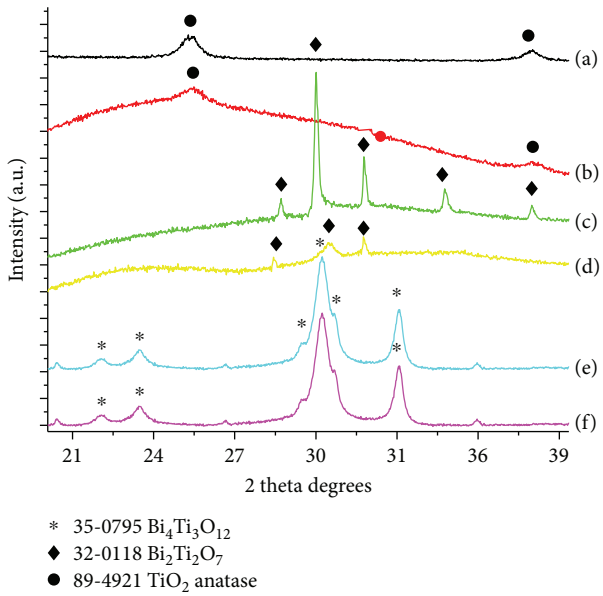

Figure 3: X-ray patterns of the TiO_2 thin films modified with several bismuth contents (a) 0, (b) 0.5, (c) 4.9, (d) 10.4, (e) 21.5, and (f) 25.4 at. %.

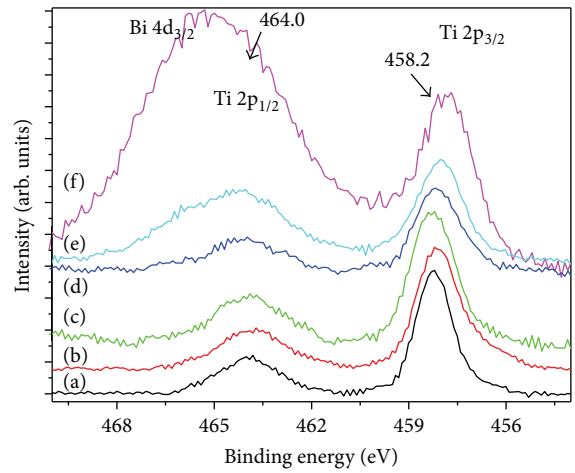

Figure 4: Ti 2p region spectra evolution as a function of bismuth content (a) 0, (b) 0.5, (c) 4.9, (d) 10.4, (e) 21.5, and (f) 25.4 at. %.

to obtain information about the interaction of the Ti atoms with the Bi and O atoms in the last atomic layer in the thin films as well as its chemical state (Figure 5). In Figure 5(a), two doublets can be observed; the first one with peaks located at 458.2 and 464.0 eV is attributed to the doublet of Ti-O bonds of the TiO_2 in its anatase phase, whereas the peaks at 456.7 and 462.9 eV could be attributed to a second doublet of Ti-O bonds in Ti_2O_3 (Figure 5(a)) [15]. The presence of Ti^{3+} due to oxygen vacancies has been reported before, resulting from the transfer of two electrons towards two adjacent Ti^{4+} to form Ti^{3+} on the surface. The spectrum of the Ti region in the sample with 10.4 at. % of bismuth (Figure 5(b) shows peaks attributed to three main doublets: the first one, located at 456.7 and 462.3 eV, is attributed to the Ti-O bonds as in Ti_2O_3; the second one, at 457.9 and 463.9 eV, has a closed binding energy than the one reported by Wang and Ma for the compounds similar to bismuth titanates, so this peaks are attributed to the Ti-Bi-O bonds in the bismuth titanate [16]; finally, the third one, with peaks located at 458.3 and 464.1 eV, could be attributed to the Ti-O bonds in the anatase phase of TiO_2. Spectrum of the thin film with bismuth content of 25.4 at. % (Figure 5(c)) shows two doublets: the first doublet at 456.7 and 462.5 eV attributed to the Ti-O bonds in the Ti_2O_3 and the second doublet at 457.9 and 464.7 eV revealing the presence of Ti-Bi-O bonds as in the bismuth titanates $Bi_4Ti_3O_{12}$. Ti $2p_{1/2}$ photoemission is overlapped in a partial way by the Bi $4d_{3/2}$ core level peak [15, 16].

Figure 6 shows the Bi 4f photoelectron spectra of the thin films displaying a characteristic doublet located at

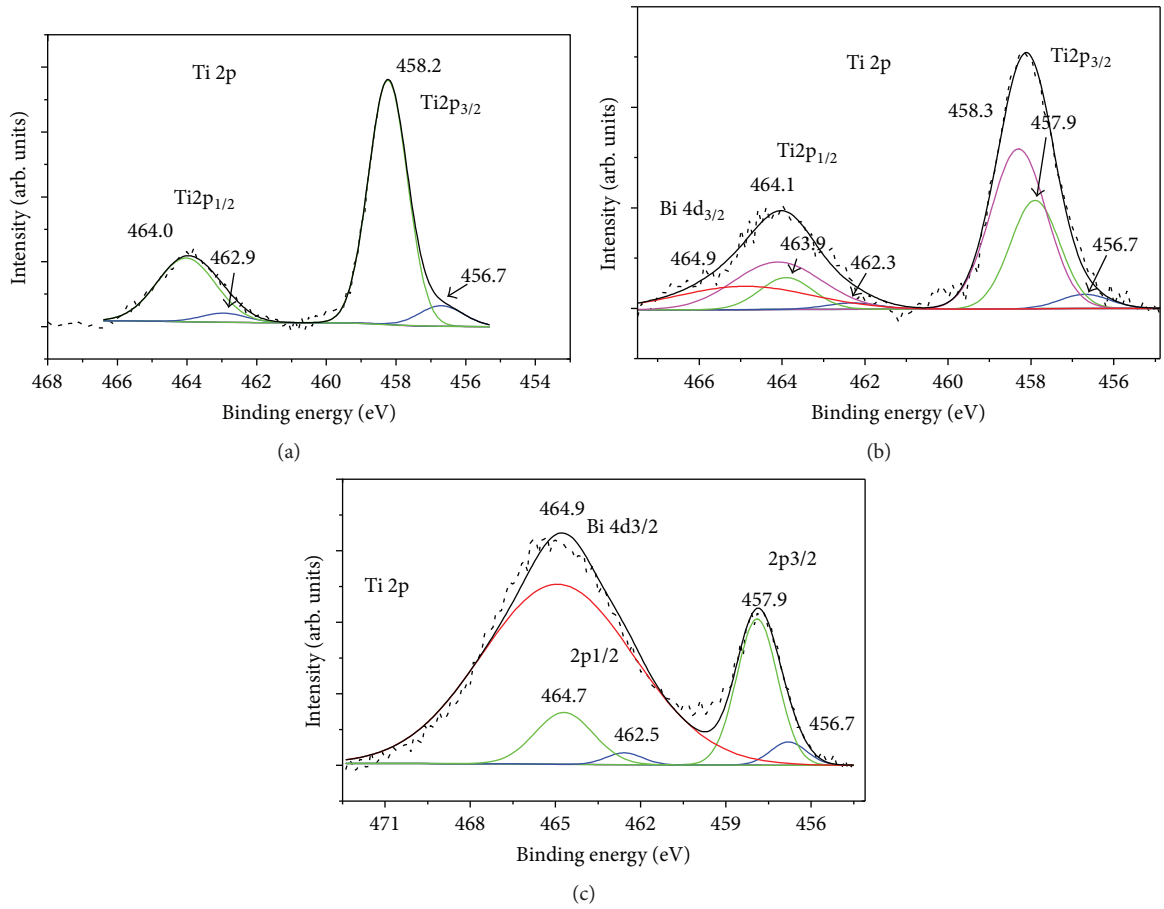

Figure 5: Gaussian deconvolution of the XPS spectra, Ti 2p region (a) 0 at. %, (b) 10.4 at. %, and (c) 25.4 at. % of bismuth.

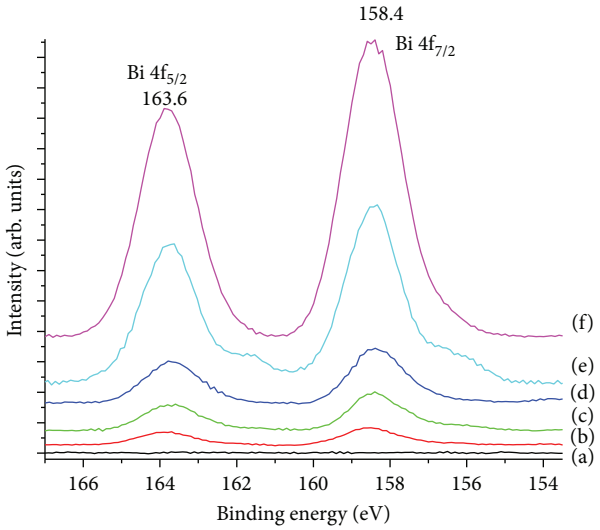

Figure 6: XPS spectra evolution of Bi 4f region as a function of bismuth content, (a) 0, (b) 0.5, (c) 4.9, (d) 10.4, (e) 21.5, and (f) 25.4 at. %.

158.4 and 163.6 eV. These signals were deconvoluted fitting two doublets: one of them located at 158.5 and 163.9 eV could be correlated to the Bi-Ti-O bonds in the layer $Bi_2Ti_3O_{10}^{2-}$ of the perovskite-type structure $Bi_4Ti_3O_{12}$ (Figure 7(a)), and the other doublet with peaks located at 156.8 and 161.9 eV could be assigned to the Bi-O bonds most probably as in the $(Bi_2O_2)^{2+}$ layer of the perovskite-type structure. These results suggest that the incorporation and further increase of Bismuth into the film changes the proportion of Bi-O bonds most probably in the $(Bi_2O_2)^{2+}$ layer, forming the perovskite structure at 21.5 at. % of Bi (Figure 7(b)). XPS spectrum of the sample with the highest bismuth content (25.4 at. %) increases the proportion of the doublet located at 158.4 and 163.8 eV correlated with the Bi-Ti-O bonds in the $Bi_4Ti_3O_{12,}$ and the other doublet with peaks located at 156.6 and 162.4 eV assigned to the Bi-O bonds in the $(Bi_2O_2)^{2+}$ layer decreases probably due to starting of the Bi_2O_3 formation (Figure 7(c)). The line shape of the O 1s core level photoemission spectra of the thin films is shown in Figures 8(a)–8(f), and it is important to remark that two peaks are clearly observed. The first peak located at the low binding energy 529.8 eV can be assigned to the Ti-O bond while the second peak located at 532.5 eV can be attributed to the oxygen bonded to bismuth [17, 18]. Jovalekić et al. have reported that oxygen atom in a stronger Ti-O bond carries a higher effective negative charge than in a weaker Bi-O bond [17]. This correlation between the effective charge of oxygen atom and the binding energy of oxygen core electrons agrees with previous reports [17, 18].

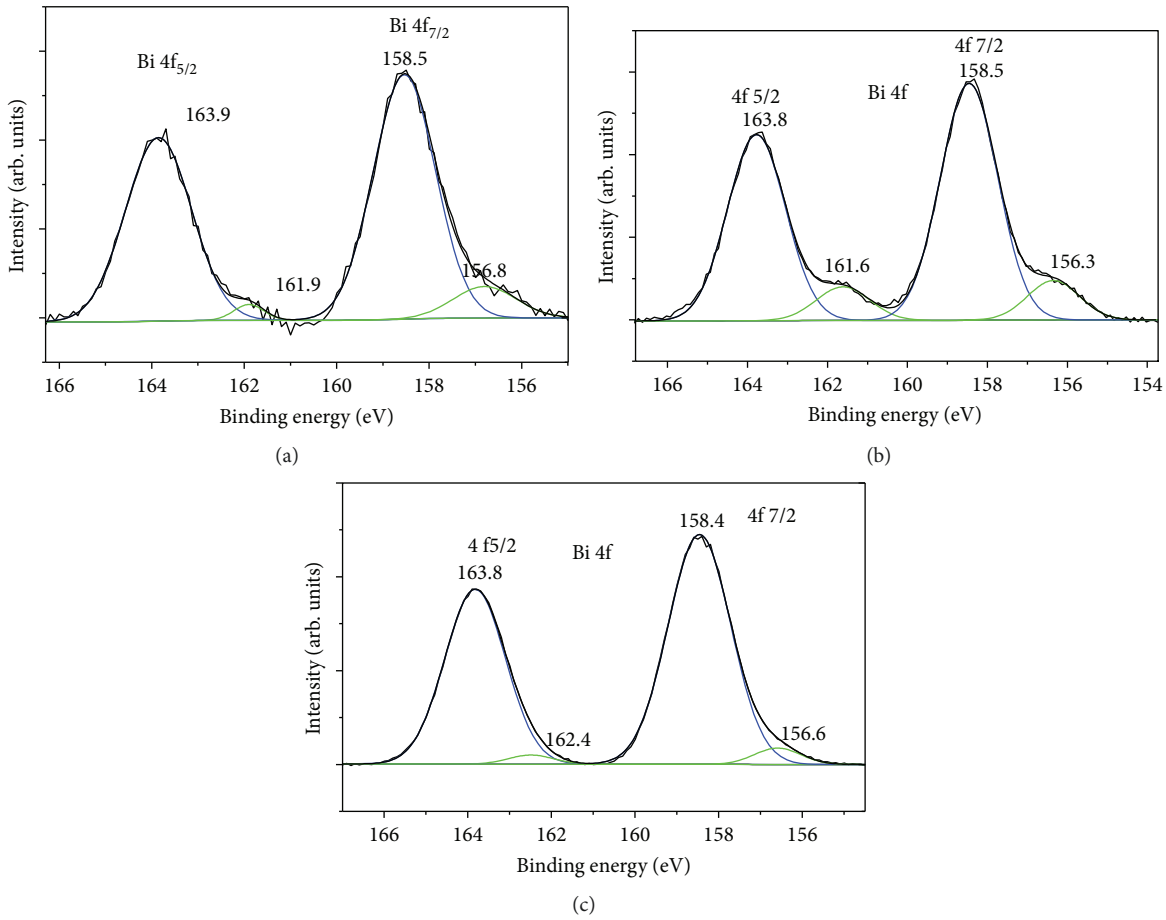

Figure 7: Gaussian deconvolution of the XPS spectra, Bi 4f7/2 region (a) 0.5, (b) 21.5, and (c) 25.4 at. % of bismuth.

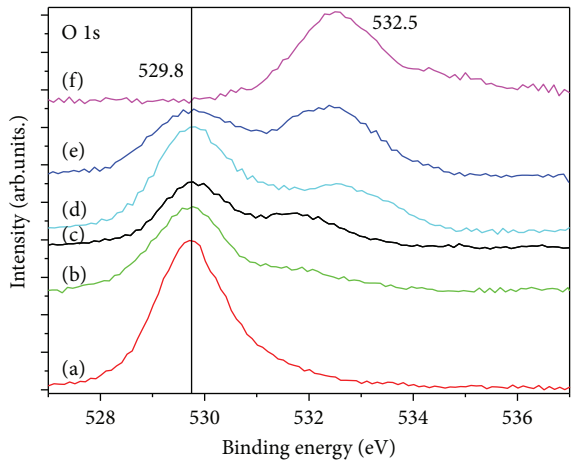

Figure 8: XPS spectra evolution of O 1s region as a function of bismuth content, (a) 0, (b) 0.5, (c) 4.9, (d) 10.4, (e) 21.5, and (f) 25.4 at. %.

3.5. Diffuse Reflectance Spectroscopy. Table 2 shows the optical band gap (Eg) values determined using the Kubelka-Munk method; this was done by transforming the reflectance spectra of the samples with different Bi contents to the Kubelka-Munk function, F(R), and then plotting $(F(R)\ E)^{1/2}$ versus E, considering a direct allowed transition band gap.

Table 2: Effect of bismuth content on the band gap energy.

Bismuth content (at. %)	Band gap energy (eV)
0	3.3
0.5	3.3
4.9	3.2
10.4	3.1
21.5	2.9
25.4	2.7

The Eg values were obtained by a linear fit of the linear portions of the curve, determining its intersection with the photon energy axis [12]. The reflectance spectra of the samples and the $(F(R)\ E)^{1/2}$ versus E graphs as well as the linear fits for estimating the band gap energy are shown in Figure 9. In these cases, the employed method allows the determination of the band gap values with good accuracy [13]. As it is observed in Table 2, the obtained results reveal that when Bi content increases in the thin films, the band gap narrows from 3.3 eV to values as low as 2.7 eV ($\lambda = 459$ nm); these low band gap values make this material potentially active under light illumination in the visible region of the electromagnetic spectrum.

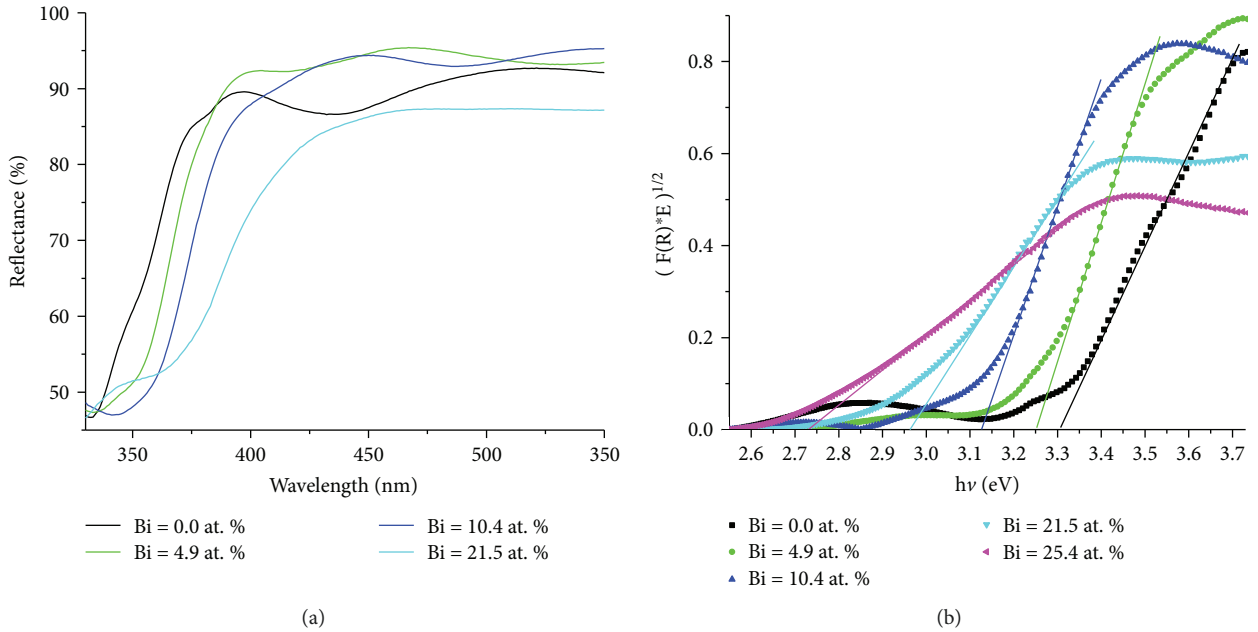

Figure 9: (a) Reflectance spectra and (b) $(F(R)\ E)^{1/2}$ versus E graphs of the prepared films.

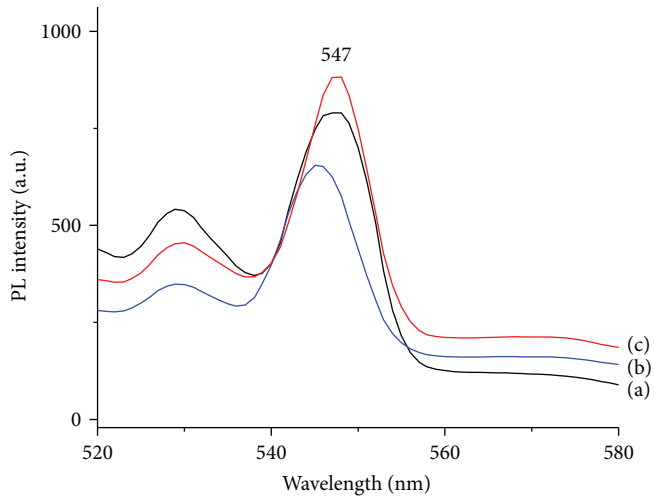

Figure 10: Photoluminescence spectra of (a) 0, (b) 21.5, and (c) 25.4 at. % of bismuth.

3.6. Photoluminescence Spectra. Figure 10 shows the photoluminescence spectra of the TiO_2 and the Bi-modified TiO_2 thin films. The PL spectrum of the TiO_2 is characterized by an intense band peaking at 547 nm. This can be interpreted as a higher electron hole recombination rate in the TiO_2 thin film as the PL intensity is related directly to the electron-hole recombination rate [19]. The same band with similar intensity is seen for the photocatalyst with 25.4 at. % of Bi. The PL intensity of the spectrum corresponding to the photocatalyst with 21.5 at. % of Bi is approximately 20% lower than the PL intensity determined as the area under the curve of the TiO_2 film, indicating that this sample exhibits the lowest recombination rate.

3.7. Photocatalytic Activity. To determine the photocatalytic activity, a photodegradation experiment of MG under simulated solar light was performed. Figure 11 shows the MG degradation degree as a function of the reaction time using thin films with different bismuth content. The MG degradation due to the photolysis process was close to 27% after 180 minutes of irradiation, and it was the lowest degradation degree as is seen in Figure 11. The TiO_2 film without bismuth behaves similarly to the photolysis process reaching a slightly higher conversion close to 34.7%. The film containing 0.5 at. % of bismuth shows a higher photocatalytic activity, of approximately 10% greater than the TiO_2 catalyst. Further increase in the Bi content, 4.9 at. %, improves in 34% the degradation degree. For a Bi content of 10.4 at. %, a decrease in the photoactivity is observed. The film with a bismuth content of 21.5 at. % improves significantly the photocatalytic activity reaching 64.6% of MG degradation after 180 min of irradiation time, 84% higher than the activity of the TiO_2

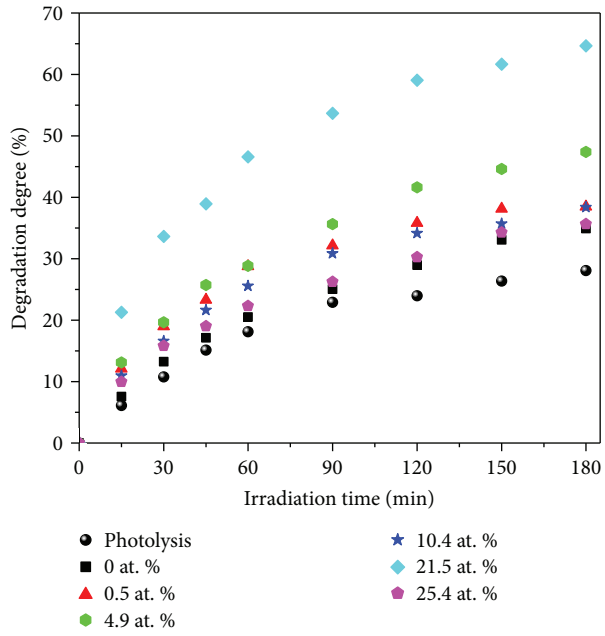

Figure 11: Photodegradation percent of MG dye using the Bi-modified TiO_2 thin films under solar simulated irradiation.

film. This enhanced photocatalytic activity could be attributed to the presence of $Bi_4Ti_3O_{12}$ as the main crystalline phase in the photocatalytic formulation as well as to the lower recombination rate of the electron-hole pairs as was suggested by the PL results. In fact, the sample with the highest Bi content diminishes the degradation degree to values nearly to the obtained using TiO_2. In general terms, thin films containing bismuth exhibit a better photocatalytic activity than pure TiO_2 thin film.

Table 3 shows the values of the kinetic constant, k_{app} (min^{-1}), obtained from a fitting of the concentration as a function of the reaction time assuming a pseudo-first order expression using a least square data treatment with an acceptable precision [20]. These values agree with the photocatalytic degradation degree reached for each thin film. Additionally, the mineralization degree was followed by the quantification of the total organic carbon (TOC) through the reaction time. The degradation degrees determined by TOC and UV-Vis measurements are quite similar as it can be seen from Table 4. This indicates that the photodegradation process follows the route of mineralization of the organic dye tested. Further studies with reactive trap molecules indicate that mineralization of MG is mainly through the electron route, specifically by the $O_2^{\bullet}$ superoxide radicals.

4. Conclusions

Bi-modified TiO_2 thin films were prepared by the sol-gel and spin coating techniques. In this way, films with Bi contents from 0.5 to 25.4 at. % were obtained. The sol-gel technique induces the Bi incorporation into the TiO_2 lattice with the consequent formation of bismuth titanate, $Bi_4Ti_3O_{12}$, at higher Bi contents. Additionally, the Bi content in the thin

Table 3: Kinetic rate constant (k_{app}) for photocatalytic formulations as a function of bismuth content, determined using a least square data treatment [20].

Bismuth content (at. %)	k_{app} (min^{-1})
Uncatalyzed	0.0029 ± 0.00006
0	0.0038 ± 0.00009
0.5	0.0038 ± 0.00009
4.9	0.0048 ± 0.00007
10.4	0.0038 ± 0.00008
21.5	0.0063 ± 0.00009
25.4	0.0036 ± 0.00006

Table 4: Mineralization degree through TOC and photodegradation percent of Malachite Green dye through UV-VIS at 180 min of irradiation time, using a solar simulator as irradiation source.

Bismuth content (at. %)	TOC (ppm)	Mineralization degree (TOC)	Degradation degree (UV-Vis)
Reference	9.2	0	0
Uncatalyzed	8.4	9.1	28.1
0	5.9	35.8	34.9
0.5	6.3	31.7	38.5
4.9	5.0	45.2	47.4
10.4	5.7	38.2	38.4
21.5	4.1	55.8	64.6
25.4	5.8	37.5	35.6

films has a strong effect on the band gap energy which decreases from 3.3 eV to values as low as 2.7 eV making these materials potentially photoactive under solar radiation. This is due to the higher wavelength required to generate the electron-hole pairs increasing the absorption spectral window of these materials. However, this lower band gap energy can be responsible for a higher recombination rate of the photogenerated charge carriers. The improved photocatalytic activity leading to the MG degradation under simulated solar light can be attributed to the $Bi_4Ti_3O_{12}$ phase at a bismuth content of 21.5 at. %.

Additional Points

Highlights. The perovskite-type structure of bismuth titanate was obtained. The incorporation of Bi makes photocatalysts active with solar radiation. Bismuth titanate, $Bi_4Ti_3O_{12}$, enhances the photocatalytic activity.

Conflicts of Interest

The authors declare that there is no conflict of interests regarding the publication of this paper.

Acknowledgments

The authors thank CONACYT for the provided equipment through the CB-168827 and CB-240998 project. The authors would like to thank Dr. Uvaldo Hernández Balderas, M. en C. Alejandra Nuñez, Dra. Melina Tapia, M. en C. Lizbeth Triana, and LIA Citlalit Martinez Soto for their technical assistance.

References

[1] M. Yasmina, K. Mourad, S. H. Mohammed, and C. Khaoula, "Treatment heterogeneous photocatalysis; factors influencing the photocatalytic degradation by TiO_2," *Energy Procedia*, vol. 50, pp. 559–566, 2014.

[2] S. Bagwasi, Y. Niu, M. Nasir, B. Tian, and J. Zhang, "The study of visible light active bismuth modified nitrogen doped titanium dioxide photocatlysts: role of bismuth," *Applied Surface Science*, vol. 264, pp. 139–147, 2013.

[3] M. Pelaez, N. T. Nolan, S. C. Pillai et al., "A review on the visible light active titanium dioxide photocatalysts for environmental applications," *Applied Catalysis B: Environmental*, vol. 125, pp. 331–349, 2012.

[4] D. A. Solis-Casados, L. Escobar-Alarcón, L. M. Gómez-Oliván, E. Haro-Poniatowski, and T. Klimova, "Photodegradation of pharmaceutical drugs using Sn-modified TiO_2 powders under visible light irradiation," *Fuel*, vol. 198, pp. 3–10, 2017.

[5] H. Cheng, B. Huang, J. Lu et al., "Synergistic effect of crystal and electronic structures on the visible-light-driven photocatalytic performances of Bi_2O_3 polymorphs," *Physical Chemistry Chemical Physics*, vol. 12, no. 47, pp. 15468–15475, 2010.

[6] W. Raza, M. M. Haque, M. Muneer, T. Harada, and M. Matsumara, "Synthesis, characterization and photocatalytic performance of visible light induced bismuth oxide nanoparticle," *Journal of Alloys and Compounds*, vol. 648, pp. 641–650, 2015.

[7] H. Zhang, M. Lü, S. Liu et al., "Preparation and photocatalytic properties of sillenite $Bi_{12}TiO_{20}$ films," *Surface and Coatings Technology*, vol. 202, no. 20, pp. 4930–4934, 2008.

[8] X. Lin, P. Lv, Q. Guan, H. Li, H. Zhai, and C. Liu, "Bismuth titanate microspheres: directed synthesis and their visible light photocatalytic activity," *Applied Surface Science*, vol. 258, no. 18, pp. 7146–7153, 2012.

[9] C. Du, D. Li, Q. He et al., "Design and simple synthesis of composite $Bi_{12}TiO_{20}/Bi_4Ti_3O_{12}$ with a good photocatalytic quantum efficiency and high production of photo-generated hydroxyl radicals," *Physical Chemistry Chemical Physics*, vol. 18, no. 38, pp. 26530–26538, 2016.

[10] R. A. Golda, A. Marikani, and D. P. Padiyan, "Mechanical synthesis and characterization of $Bi_4Ti_3O_{12}$ nanopowders," *Ceramics International*, vol. 37, no. 8, pp. 3731–3735, 2011.

[11] D. A. Solís-Casados, L. Escobar-Alarcón, A. Arrieta-Castañeda, and E. Haro-Poniatowski, "Bismuth–titanium oxide nanopowders prepared by sol–gel method for photocatalytic applications," *Materials Chemistry and Physics*, vol. 172, pp. 11–19, 2016.

[12] A. Murphy, "Band-gap determination from diffuse reflectance measurements of semiconductor films, and application to photoelectrochemical water-splitting," *Solar Energy Materials and Solar Cells*, vol. 91, no. 14, pp. 1326–1337, 2007.

[13] R. López and R. Gómez, "Band-gap energy estimation from diffuse reflectance measurements on sol–gel and commercial TiO_2: a comparative study," *Journal of Sol-Gel Science and Technology*, vol. 61, no. 1, pp. 1–7, 2012.

[14] E. Haro-Poniatowski, R. Rodríguez-Talavera, H. M. de la Cruz, O. Cano-Corona, and R. Arroyo-Murillo, "Crystallization of nanosized titania particles prepared by the sol-gel process," *Journal of Materials Research*, vol. 9, no. 08, pp. 2102–2108, 1994.

[15] C. Jovalekic, M. Zdujic, and L. J. Atanasoska, "Surface analysis of bismuth titanate by Auger and X-ray photoelectron spectroscopy," *Journal of Alloys and Compounds*, vol. 469, no. 1-2, pp. 441–444, 2009.

[16] L. Wang and W. Ma, "$Bi_4Ti_3O_{12}$ synthesized by high temperature solid phase method and it's visible catalytic activity," *Procedia Environmental Sciences*, vol. 18, pp. 547–558, 2013.

[17] Č. Jovalekić, M. Pavlović, P. Osmokrović, and L. J. Atanasoska, "X-ray photoelectron spectroscopy study of $Bi_4Ti_3O_{12}$ ferroelectric ceramics," *Applied Physics Letters*, vol. 72, no. 9, pp. 1051–1053, 1998.

[18] Z. Hu, H. Gu, Y. Hu, Y. Zou, and D. Zhou, "Microstructural, Raman and XPS properties of single-crystalline $Bi_{3.15}Nd_{0.85}Ti_3O_{12}$ nanorods," *Materials Chemistry and Physics*, vol. 113, no. 1, pp. 42–45, 2009.

[19] P. Malathy, K. Vignesh, M. Rajarajan, and A. Suganthi, "Enhanced photocatalytic performance of transition metal doped Bi_2O_3 nanoparticles under visible light irradiation," *Ceramics International*, vol. 40, no. 1, pp. 101–107, 2014.

[20] G. Lente, *Deterministic Kinetics in Chemistry and Systems Biology*, Springer, London, UK, 2015.